



**HAL**  
open science

# The role of nitrogen in the oxidation behaviour of a Ti6242S alloy: a nanoscale investigation by atom probe tomography

Charlotte Dupressoire, Marion Descoins, Aurélie Vande Put, Enrica Epifano, Dominique Mangelinck, Philippe Emile, Daniel Monceau

## ► To cite this version:

Charlotte Dupressoire, Marion Descoins, Aurélie Vande Put, Enrica Epifano, Dominique Mangelinck, et al.. The role of nitrogen in the oxidation behaviour of a Ti6242S alloy: a nanoscale investigation by atom probe tomography. *Acta Materialia*, 2021, 216, pp.117134. 10.1016/j.actamat.2021.117134 . hal-03431660

**HAL Id: hal-03431660**

**<https://hal.science/hal-03431660>**

Submitted on 16 Nov 2021

**HAL** is a multi-disciplinary open access archive for the deposit and dissemination of scientific research documents, whether they are published or not. The documents may come from teaching and research institutions in France or abroad, or from public or private research centers.

L'archive ouverte pluridisciplinaire **HAL**, est destinée au dépôt et à la diffusion de documents scientifiques de niveau recherche, publiés ou non, émanant des établissements d'enseignement et de recherche français ou étrangers, des laboratoires publics ou privés.



Distributed under a Creative Commons Attribution - NonCommercial - NoDerivatives 4.0 International License







## Open Archive Toulouse Archive Ouverte (OATAO)

OATAO is an open access repository that collects the work of Toulouse researchers and makes it freely available over the web where possible

This is an author's version published in: <http://oatao.univ-toulouse.fr/28480>

**Official URL:** <https://doi.org/10.1016/j.actamat.2021.117134>

### To cite this version:

Dupressoire, Charlotte  and Descoins, Marion and Vande Put, Aurélie  and Epifano, Enrica  and Mangelinck, Dominique and Emile, Philippe and Monceau, Daniel  *The role of nitrogen in the oxidation behaviour of a Ti6242S alloy: a nanoscale investigation by atom probe tomography.* (2021) Acta Materialia, 216. 117134. ISSN 1359-6454

Any correspondence concerning this service should be sent to the repository administrator: [tech-oatao@listes-diff.inp-toulouse.fr](mailto:tech-oatao@listes-diff.inp-toulouse.fr)

# The role of nitrogen in the oxidation behaviour of a Ti6242S alloy: a nanoscale investigation by atom probe tomography

C. Dupressoire<sup>a</sup>, M. Descoins<sup>b</sup>, A. Vande Put<sup>a</sup>, E. Epifano<sup>a</sup>, D. Mangelinck<sup>b</sup>, P. Emile<sup>c</sup>, D. Monceau<sup>a,\*</sup>

<sup>a</sup>CIRIMAT laboratory, University of Toulouse, CNRS, INPT, UPS, ENSIACET 4 allée Emile Monso, BP-44362, 31030 Toulouse Cedex 4, FRANCE

<sup>b</sup>Aix-Marseille Université, CNRS, IM2NP, Faculté de Saint-Jérôme, Case 142, 13397 Marseille Cedex 20, FRANCE

<sup>c</sup>Airbus Operations SAS, 316 Route de Bayonne, 31060 Toulouse Cedex 09, France

## ARTICLE INFO

### Keywords:

Titanium-based alloy  
Oxidation  
Oxygen dissolution  
Nitrogen  
Atom probe tomography

## ABSTRACT

When used at high temperature in air, titanium-based alloys form an oxide scale at their surface but also dissolve large amount of oxygen in their metallic matrix and this is a cause of embrittlement. Nitrogen is a secondary oxidant, which also dissolves in and embrittles the alloy. Oxidation experiments of Ti-6Al-2Sn-4Zr-2Mo-0.1Si titanium-based alloy, for 1000 h at 650 °C in synthetic air (N<sub>2</sub>-20%O<sub>2</sub>) and in a mixture of Ar-20%O<sub>2</sub>, showed that nitrogen decreases both oxide scale growth and oxygen dissolution. Atom probe tomography was used to investigate the alloy/oxide interface. The results revealed that the nitrogen effect is due to the formation of interfacial layers of oxynitrides and nitride (Ti<sub>2</sub>N), but also to the formation of a nitrogen rich  $\alpha$ -titanium-based solid solution, which all act as diffusion barriers for oxygen, because of their low oxygen solubility. A comparison between the experimental results and thermodynamic calculations is also reported.

## 1. Introduction

Ti-based alloys compete with Ni-based superalloys in the aeronautic industry, because of their excellent specific strength. However, they are limited to low or moderate temperatures (<500°C-600°C) applications because of creep but also because of environmental embrittlement. As in-service temperatures are increasing in order to improve the efficiency of engines, the high temperature behaviour of Ti-alloys need to be improved. The Ti-O system is quite complex, as shown by the phase diagram in Fig. 1, where several oxides are reported. The rutile TiO<sub>2</sub> is the stable phase for the oxygen partial pressure conditions of common atmospheres and this oxide is found on the surface of oxidized Ti-based alloys. In addition to the oxide scale formation, oxygen dissolution takes place within Ti-based alloys. Indeed, about 33 at.% of oxygen can be dissolved in the low temperature  $\alpha$ -Ti phase and up to 12 at.% can be dissolved in the high temperature  $\beta$ -Ti form (Fig. 1). The formation of an oxygen-rich solid solution below the oxide scale is generally referred in the literature as “oxygen rich layer” (ORL) or “ $\alpha$ -case” [1]. Nevertheless, the term “ $\alpha$ -case” should be used

only for oxidation at very high temperature, when oxygen dissolution leads to the  $\beta \rightarrow \alpha$  transition under the surface. At moderate temperatures for aeronautic applications (<650 °C), oxygen dissolution under the surface does not affect much the  $\alpha$  volume fraction. However, oxygen dissolution leads to a loss of ductility [2,3], which can be detrimental to fatigue resistance [1].

Moreover, titanium alloys can form nitrides and dissolve up to 23 at.% nitrogen, for temperatures higher than 1060°C [4], as shown in Fig. 2 (Ti-N phase diagram computed with the TCT11 database from Thermo-Calc). In air, titanium oxides are much more stable than nitrides, as shown by the predominance diagram at 650 °C in Fig. 3 (similar results are found at all temperatures). Therefore, in agreement with experimental evidences, TiO<sub>2</sub> is expected to form on the surface of the Ti-based alloys.

It has been shown previously that nitrogen decreases oxidation kinetics of Ti and Ti-based alloys [5,6]. Ti6242S commercial alloy exposed to Ar-20%O<sub>2</sub> and to synthetic air (N<sub>2</sub>-20%O<sub>2</sub>) for 100 h at 650 °C, showed that a N-rich environment lead to a thinner and more compact oxide scale [6]. This was accompanied by a lower oxygen content in the alloy, at several micrometers under the alloy/oxide interface, as measured by electron probe microanalysis (EPMA). As a consequence, a lower overall oxygen dissolution was observed within the alloy. Chaze and Coddet proposed three possible explanations to the positive influence of nitrogen on the oxida-

\* Corresponding author.

E-mail address: daniel.monceau@toulouse-inp.fr (D. Monceau).

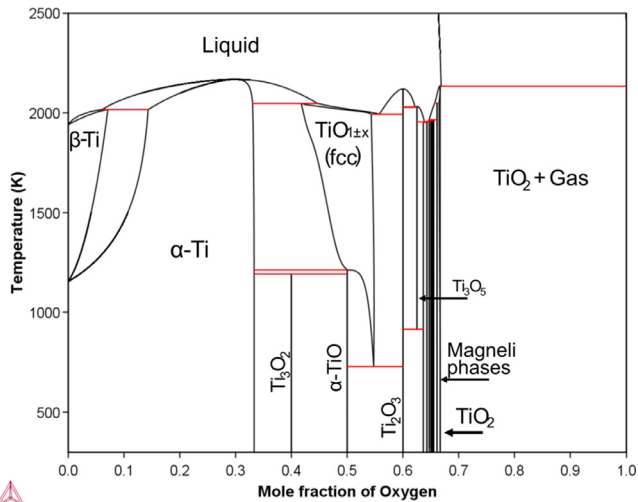


Fig. 1. Ti-O binary phase diagram (computed with the TCTI1 database from Thermo-Calc).

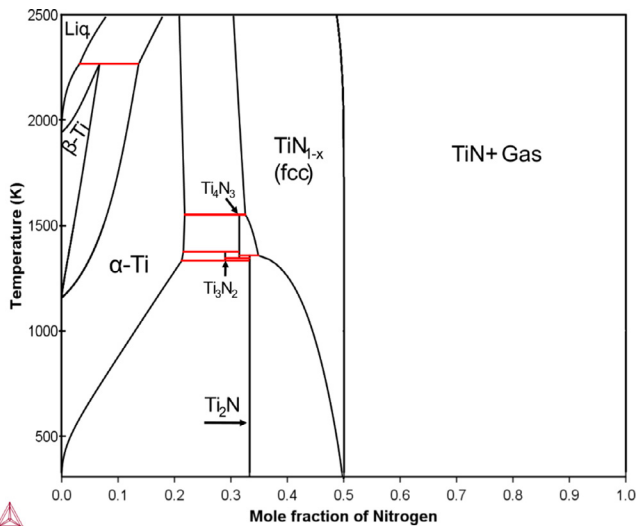


Fig. 2. Ti-N binary phase diagram (computed using the TCTI1 database from Thermo-Calc).

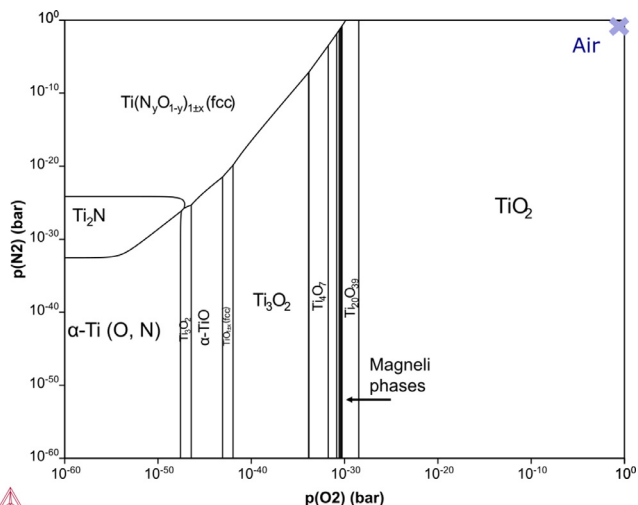


Fig. 3. Predominance diagram at 650 °C for the Ti-O-N system (computed using the TCTI1 database from Thermo-Calc).

tion of Ti and Ti-X alloys ( $X = \text{Al, Cr, Si}$ ) [5]. They consider that nitrogen would be incorporated in solution in the rutile layer. As nitrogen diffuses faster in rutile than in titanium [7], nitrogen should accumulate in the oxide, next to the alloy/oxide interface. Chaze and Coddet suggest that nitrogen could decrease the concentration of oxygen vacancies in the oxide and this would decrease the driving force for oxygen transport in the rutile layer [5]. However, this is in contradiction with Density Functional Theory (DFT) calculations revealing that N doping of rutile would increase oxygen vacancies concentration [8]. The second possible explanation given by Chaze and Coddet was that N could decrease the O solubility limit within the metal. Consequently, the inward oxygen flux towards the metal bulk would be lower [5,9]. The third proposed explanation was the formation of a nitride at the alloy/oxide interface. Indeed, as shown in Fig. 3, at the Ti/oxide interface, the oxygen partial pressure ( $p_{\text{O}_2}$ ) can be low enough to stabilize an oxynitride and a nitride. The formation of such a protective inner nitride layer was reported for binary alloys such as Ti-Cr and Ti-Si alloys, for which it was claimed that chromium and titanium nitrides were detected by X-Ray Diffraction (XRD) respectively, but no XRD diagram was given by authors [10,11]. However, nitrides were observed thanks to optical microscopy as a thin gold layer in Ti-based intermetallics  $\text{Ti}_3\text{Al}$  [12] and this is often reported in TiAl, e.g. [13]. The formation of a  $\text{Ti}_2\text{N}$  nitride was detected by XRD after 5 h oxidation in air at 700°C of shot peened Ti CP grade 1 samples. Nuclear reaction analysis (NRA) of these samples revealed a continuous nitrogen enrichment below the oxide scale [14]. No other study was found in the literature to explain the nitrogen effect on the oxidation behaviour of  $\alpha$  or  $\alpha$ - $\beta$  titanium-based alloys.

To this aim, it is necessary to measure the nitrogen and oxygen dissolutions next to the alloy/oxide interface. The phase transformation(s) that these elements can induce need to be observed and understood. Most studies dedicated to titanium oxidation characterization make use of micro-hardness or EPMA concentration profiles, but these techniques do not have sufficient spatial and chemical resolutions. In a recent work by our group, the Electron Energy Loss Spectroscopy (EELS) in a Scanning Transmission Electron Microscope (STEM) was used to study the alloy/oxide interface of the same Ti6242S alloy, after oxidation in both Ar20% $\text{O}_2$  and synthetic air, at 650 °C [15]. To complete that study, atom probe tomography (APT) is proposed here as a possible mean to get a chemical analysis at the atomic scale. APT is a 3D microscopy technique with a unique combination of spatial and chemical resolution, suitable for interface investigations. This technique has already been applied to investigate the  $\alpha/\beta$  interface in TA6V alloys manufactured by electron beam melting [16–18]. It was shown in these studies that APT can measure oxygen, nitrogen and carbon concentrations inferior to 0.05 at% [16]. Several studies used APT to investigate fine scale precipitations in Ti-based alloys [19–22]. APT has also been applied to O dissolution in pure Ti [23–26]. A TA6V alloy in the  $\alpha/\beta$  phase field was exposed to air (the temperature is not clearly stated in the paper). An increase in hardness was observed and oxygen (1 wt.%) and nitrogen (0.4 wt.%) contents were determined by APT [24]. Yan *et al.* combined TEM and APT studies to show the microstructural changes associated to the loss of ductility of the TA6V alloy when the O concentration exceeds 0.33 wt.% [23]. Gardner *et al.* investigated the effect of low O contents ( $\leq 0.49$  wt.%) on the precipitation of the  $\alpha_2$ - $\text{Ti}_3\text{Al}$  phase in a Ti-7wt.%Al alloy aged at 550°C [26]. These three APT studies concerned relatively low oxygen concentrations ( $\leq 1$  wt.%). However, during operation in oxidizing conditions, the oxygen concentration in the metal can reach up to  $\approx 33$  at.%. Only one work from Bagot *et al.* reported the application of the APT technique on the subsurface of an oxidized TA6V alloy (oxidation 24 h at 800°C in air), where O concentrations up to 25 at.% were observed [25]. However, this study concerned a region located more than 10  $\mu\text{m}$  below the oxide and,

**Table 1**  
Chemical composition of Ti6242S alloy.

Element	Ti %	Al	Sn	Zr	Mo	Si	O ppm	N	C	S	H
In weight	Bal.	6.0	1.8	4.0	2.1	0.1	1200	<5	26	8.2	44
In atoms	Bal.	10.5	0.7	2.1	1.0	0.2	3550	<17	103	12	2062

at this distance from the scale, the nitrogen was barely observed<sup>1</sup>. Indeed, the penetration depth observed for oxygen is much higher than that of nitrogen [25].

To our knowledge, APT has never been used to characterize the alloy/oxide interface in Ti-based alloys, in which O and N dissolutions can reach up to 33 at.% and 23 at.%, respectively, in the metal. This analysis is challenging as both the alloy and the oxide are expected to be insulating and very brittle in the interfacial region. In this work, we report a successful APT characterization of the alloy/oxide interface. The distribution of the alloying elements of Ti6242S alloy, and of O and N coming from the environment were determined at the alloy/oxide interface and just below this interface. These observations were done on samples oxidized in atmosphere containing 20 vol.% of O<sub>2</sub>, with or without N<sub>2</sub>. These APT analyses help to understand the role of nitrogen on the oxidation of Ti6242S alloy and show the feasibility of such analyses for other alloys and other oxidation conditions.

## 2. Methods

### 2.1. Experimental

The studied material was the near  $\alpha$ -Ti6242S Ti-based alloy. It was forged by Aubert and Duval (Pamiers, France). A solution heat treatment of 1 hour and 45 minutes at 985°C was followed by a blast air cooling and an ageing at 593°C for 9 hours. The chemical composition was determined by energy dispersive X-ray spectroscopy (EDX) for major elements and by instrumental gas analyses (IGA) for gas-forming elements (detection limits (wt): 0.5 ppm for hydrogen, 5 ppm for carbon, nitrogen and sulphur, 10 ppm for oxygen) by Evans Analytical Group (Tournefeuille, France), Table 1. Reported scanning electron microscopy (SEM) observations were done after etching in Kroll's solution (2.5 vol.% HNO<sub>3</sub>, 1.4 vol.% HF, bal. H<sub>2</sub>O). The backscattered electron (BSE) mode was used to reveal compositional contrast. A duplex microstructure was observed consisting of lamellar and globular  $\alpha$  phase (dark in SEM-BSE image) in a thin  $\beta$  phase (light in SEM-BSE image) (Fig. 4).

Samples were cut from the center of the large (tens of centimeters) ingots as thin plates of 15 × 10 × 1 mm<sup>3</sup>. Before oxidation, the samples were ground using P240 SiC grinding paper, in order to remove completely the previously formed oxide layer and to obtain equal rugosity, and they were cleaned with acetone and ethanol under ultrasounds. Just before and after oxidation, they were weighed three times using a SARTORIUS GENIUS (ME2156P) balance with an accuracy of 20 µg. Oxidation treatments were performed in a symmetrical thermobalance SETARAM TAG 24s for 100 h at 650 °C, in flowing Ar-20%O<sub>2</sub> and in flowing synthetic air. The sensitivity of the thermobalance is 0.1 µg. After these first 100 h in the TGA apparatus, the oxidation treatments were prolonged to 1000 h in an oxidation furnace at the same temperature and in the same atmosphere than in the TGA. In both cases (thermobalance and furnace), the temperature was controlled using an S-type

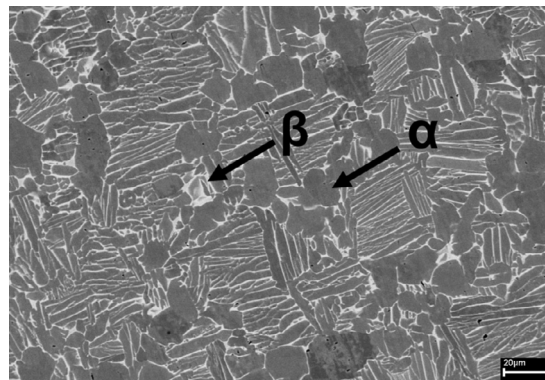


**Fig. 4.** SEM observation of Ti6242S microstructure (BSE mode).

thermocouple next to the sample. Similar gas velocities were used. A gas flux of 8.5 ml/min was set in the TGA, corresponding to a gas velocity of 0.45 mm/s. For long-term oxidations, the gas flux was set to 100 ml/min and 51 ml/min which was equivalent to 0.25 mm/s and 0.12 mm/s for synthetic air and Ar-20%O<sub>2</sub> respectively. Mass variations were measured three times after several exposure durations using the SARTORIUS GENIUS balance.

APT characterizations were performed at IM2NP (Marseille, France). Specimens were prepared from oxidized samples using a focused ion beam (FIB) on a FEI HELIOS 600i dual beam, using lift-out technique at IM2NP [27]. A platinum coating was realized in order to protect the analyzed region. The micro-tips were obtained using the annular milling method [28]. The end radius was about 100 nm. APT analyses were carried out with a LEAP 3000x HR at a temperature of 40 K and using a 100 kHz picosecond laser pulse with an energy between 0.5 and 1.2 nJ. IVAS 3.6.2 software was chosen to reconstruct data. The atoms maps were reconstructed using the tip profile option of the IVAS : this reconstruction mode used a SEM image of the tip shape after the FIB preparation to reconstruct the APT volume. Three specimens per atmosphere were successfully analysed.

Complementary characterizations of the alloy/oxide interface using Electron Probe Microscopy Analysis (EPMA) and Transmission Electron Microscopy (TEM) are also shown. EPMA was performed with a CAMECA SXFive microprobe working at 15 kV and 20 nA. The spatial resolution of the EPMA is 2-3 µm. The procedures for sample preparation and data analysis are described in a previous paper [6]. The determination of O concentration using EPMA requires a correction because of the native oxide layer always present at the surface [6]. The TEM analysis was performed using a JEOL cold-FEG JEM-ARM 200 F microscope, operating at 200 kV and equipped with a Cs corrector probe of 0.078 nm spatial resolution. Energy dispersive X-ray (EDX) was used to determine O and N contents at the alloy/oxide interface.

### 2.2. Thermodynamic calculations

Thermodynamic equilibrium calculations were performed using the TCTI1 database and Thermo-Calc software, in order to

<sup>1</sup> Nitrogen was observed only on the top (oxide side) of one of the three samples examined by Bagot *et al.* [25]. The chemical form of the nitrogen-containing region is not clearly identified, but supposed to be a mixture of nitrogen-stabilized  $\alpha$ -Ti and Ti<sub>2</sub>AlN.

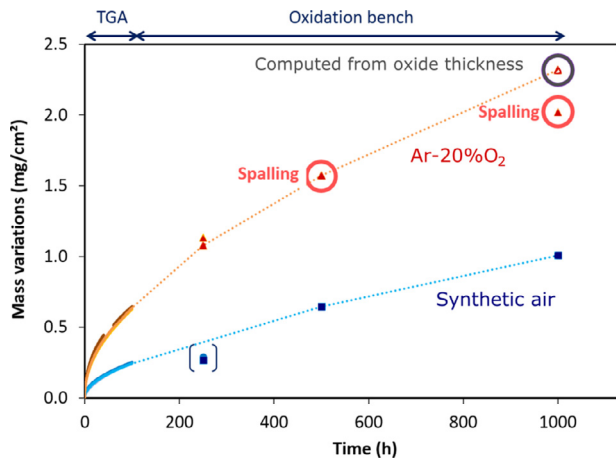


**Fig. 5.** Mass variation vs time for Ti6242S alloy oxidized at 650 °C in flowing synthetic air and Ar-20%O<sub>2</sub> gas mixture (error bars are smaller than symbol sizes).

test its prediction abilities in this system containing large amount of oxygen and nitrogen. The TCTI1 thermodynamic database was developed according to the CALPHAD method, which is a semi-empirical approach for the calculation of phase diagrams and thermodynamic properties [29]. One of the strengths of the CALPHAD method is the possibility to extrapolate the assessment of subsystems to multicomponent alloys. However, being a semi-empirical method, the reliability of CALPHAD databases is dependent on the number of assessed subsystems and on the quantity/quality of data available for the optimization of each subsystem. Concerning the elements present in the Ti6242S alloy, all the Ti-X binaries are assessed in the TCTI1 database, with the exception of X = H and S, since these two elements are not at all included in the database. In addition, it has to be noted that the ternary Ti-N-O system is not assessed, but it is obtained from the extrapolation of the Ti-O and Ti-N binaries.

### 3. Results and discussion

#### 3.1. Oxidation behaviour

Fig. 5 shows the mass changes obtained after oxidation at 650 °C in Ar-20%O<sub>2</sub> and in synthetic air. The uncertainty on the mass change values ranges between 0.008 and 0.01 mg/cm<sup>2</sup>, therefore error bars are smaller than symbol sizes. It can be seen that the mass variations obtained in synthetic air after 1000 h at 650 °C

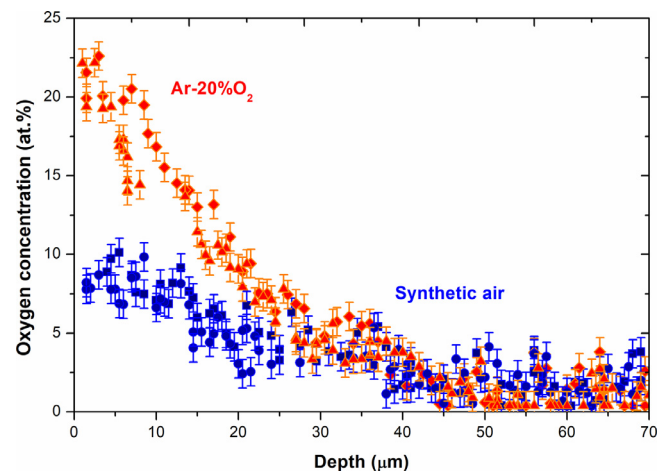


**Fig. 7.** EPMA profiles for oxygen for Ti6242S alloy oxidized at 650°C for 1000 h in flowing synthetic air (2 profiles in blue squares and circles) and Ar-20%O<sub>2</sub> (2 profiles in red triangles and diamonds)

are about 2.3 times lower than those obtained after oxidation in Ar-20%O<sub>2</sub>, i.e. with the same oxygen partial pressure but without N<sub>2</sub> (Fig. 5). This confirms our previous observations after 100 h exposures [6].

The oxide scale formed in Ar-20%O<sub>2</sub> is much thicker than the oxide scale formed in air (Fig. 6). Moreover, it is layered, whereas it is not the case when oxidation is performed in synthetic air. This layered morphology is a common feature for the TiO<sub>2</sub> growth on pure titanium and it is generally attributed to high stresses due to a large Pilling and Bedworth ratio [6]. This layered morphology was already visible at shorter oxidation times (100 hours) and discussed in more detail elsewhere [6]. An important point is that O concentration in the alloy at the alloy/oxide interface was 2 to 3 times higher in the Ar-20%O<sub>2</sub> than in synthetic air (Fig. 7). These are the results of several measurements by EPMA, a few micrometers away from the interface.

The oxidation kinetics measured in this study, in air, are in agreement with a recent review of the oxidation kinetics of Ti6242 and TA6V [30]. This is true for mass gains and for oxide layer thicknesses. Our results are similar to the slowest kinetics observed in the literature. This is in agreement with the low gas velocity used in our study, as explained in [30].

The mass gains associated to oxygen dissolution was calculated by integration of the EPMA oxygen concentration profiles. The mass gains associated with the oxide scales were calculated

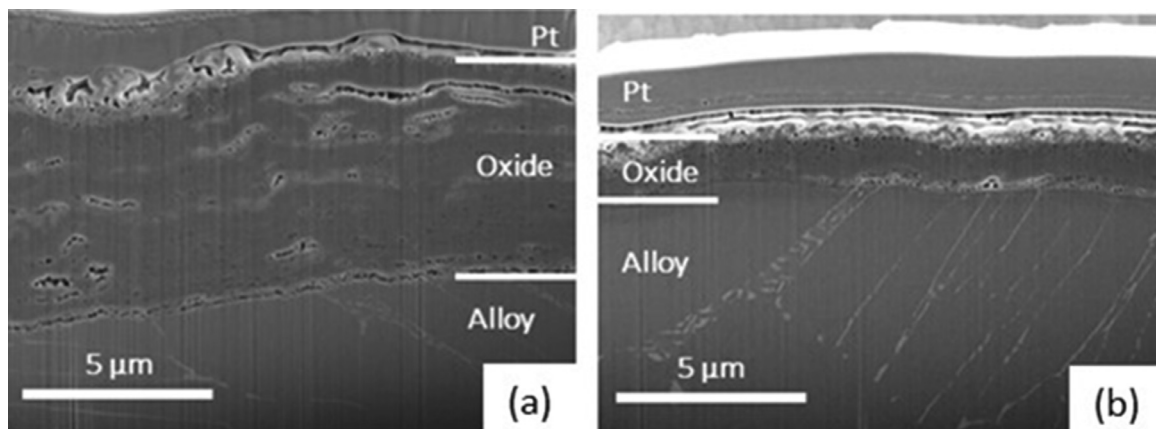


**Fig. 6.** Cross-sections (SEM-BSE) of Ti6242S alloy oxidized at 650 °C for 1000 h in flowing (a) Ar-20%O<sub>2</sub> gas mixture (b) synthetic air.

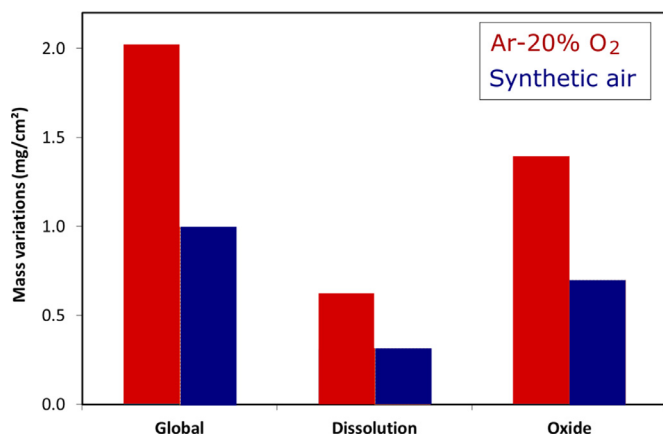


**Fig. 8.** Mass variations associated to global oxidation kinetics, to oxygen dissolution in the alloy calculated by integration of the EPMA oxygen concentration profiles and to oxide scale growth calculated by difference of the two preceding quantities. Ti6242S alloy oxidized at 650 °C for 1000 h in flowing synthetic air and Ar-20%O<sub>2</sub> gas mixture.

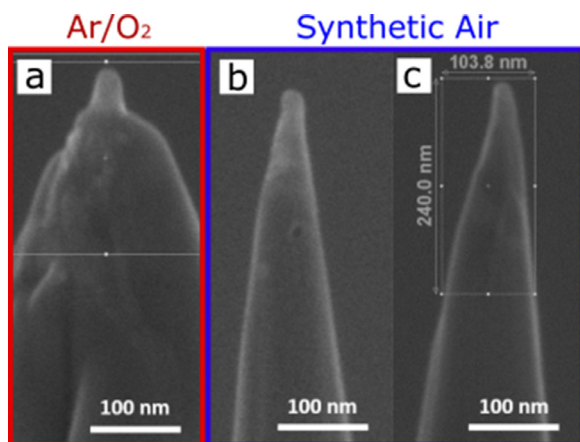


**Fig. 9.** SEM (secondary electron mode) observations of micro-tips obtained by FIB and analysed by APT for Ti6242S alloy oxidized 1000 h at 650 °C in flowing (a) Ar-20%O<sub>2</sub>, (b) and (c) synthetic air.

as the difference between the total mass gains and the one corresponding to O dissolution in the metal. To check the calculations, the mass gains due to the external scales growth were also estimated from their thickness. The mass gains associated to the oxide scale growth and to the oxygen dissolution in the metal are both lower in synthetic air than in Ar-20%O<sub>2</sub> (Fig. 8). These results confirm the observations previously made after 100h oxidation in our previous study [6]. These findings motivated us to perform further characterizations of the interfacial area with a higher spatial resolution, in order to better characterize and to improve our understanding of the nitrogen effect on the oxidation behaviour.

### 3.2. Characterization of the alloy/oxide interface

Six micro-tips were prepared by FIB, three for each atmosphere. All the tips were successfully prepared and analysed by APT. The results obtained were similar for the tips corresponding to a given atmosphere. Therefore only one specimen for the Ar-20%O<sub>2</sub> environment and two specimens for synthetic air are presented in this paper. Fig. 9 shows these three micro-tips. The APT reconstruction volumes are given in Fig. 10. For clarity, only one or two major elements are shown in the reconstructions, while the complete el-

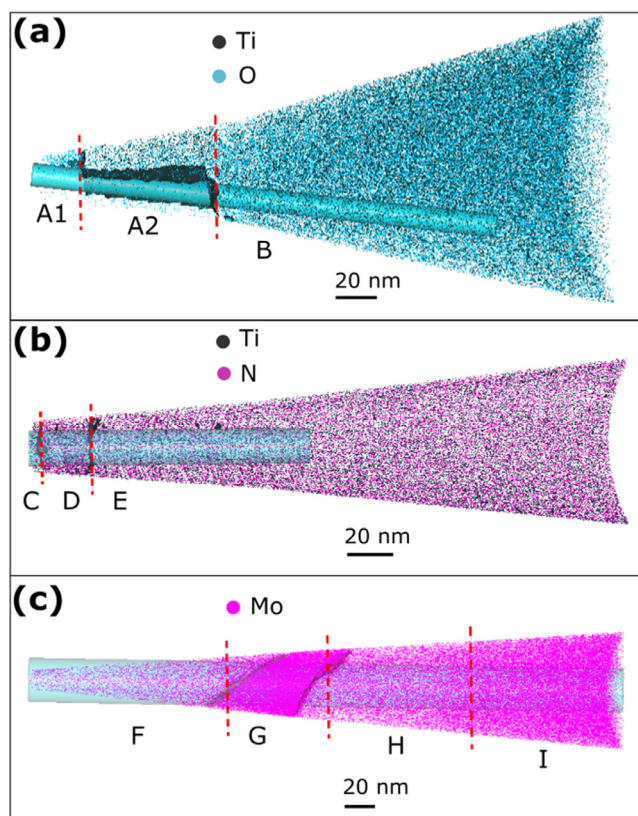


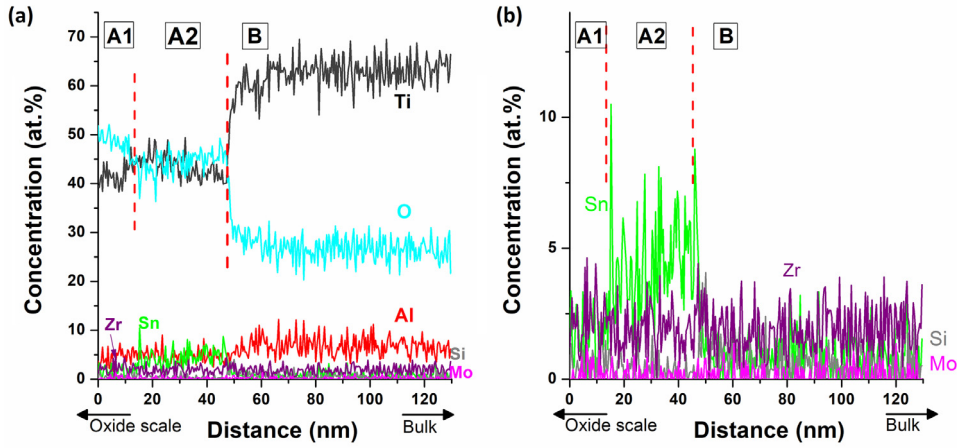
**Fig. 10.** APT reconstruction volumes for the three micro-tips: (a) Ar-20%O<sub>2</sub>, (b) and (c) synthetic air. The iso-concentration surfaces shown in the tips represent: 19 at.% Ti in (a); 36 at.% (zones C and D) and 56 at.% (zones D and E) in (b); 15 at.% Mo. The light-blue cylinders are the volume analysed to obtain the concentration profiles.

emental maps are provided in the appendices (Fig. A2, Fig. A3, Fig. A4).

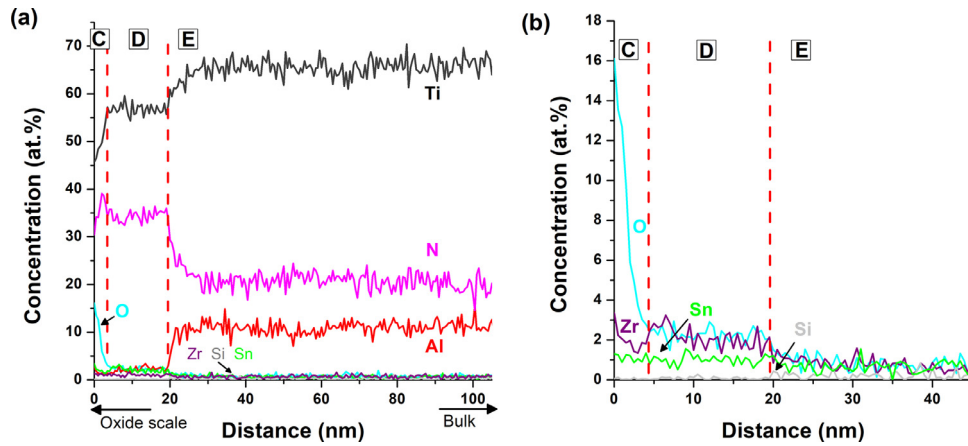
For each specimen, concentration profiles were calculated from the APT data by summing the number of atoms in cylinders taken perpendicular to the alloy/oxide interface, as shown in Fig. 10.

Fig. 11 shows the analyses related to the Ar-20%O<sub>2</sub> exposure. Two main zones were observed in the micro-tips corresponding to this atmosphere. The first one, zone A, corresponds to the minor oxides close to the alloy/ TiO<sub>2</sub> oxide interface. It is rich in titanium and oxygen. Two sub-zones could be observed: zone A1, with a measured oxygen concentration of 49 at.%, and zone A2, with 40-45 at.% O. Comparing with the Ti-O phase diagram, Fig. 1, A1 could correspond to the monoclinic  $\alpha$ -TiO [31] or to the FCC  $\beta$ -TiO<sub>1±x</sub> phase, while A2 could be mainly composed of Ti<sub>3</sub>O<sub>2</sub>. An increase of the Sn concentration is also observed in this A2 region. In a previous study, the Sn-rich Ti<sub>3</sub>(Al<sub>0.5</sub>Sn<sub>0.5</sub>) phase was observed at the alloy/oxide interface of a Ti6242S alloy coated with an Al<sub>2</sub>O<sub>3</sub> layer, after long (5000 hours) oxidation at 600°C [32]. In this case, the increase of the Sn concentration could be due to the local formation of this phase: indeed, the Al and Sn concentrations are very close in the A2 region.

The second zone, named B, was mainly composed of Ti, O and Al. The oxygen content (29 at.%) is close to the theoretical solubility limit of 33 at.% in pure titanium, Fig. 1. The aluminium concentration in zone B is about 8 at.% which is close to, but lower than the one of the alloy. Because of this concentration in O and Al, and the fact that only little  $\beta$ -Ti-gene element Mo is detected at this location, this phase should be the HCP  $\alpha$ -Ti phase saturated in oxygen. This phase will be noted  $\alpha$ -Ti(O) in this paper. However, it has to be noted that due to the Ti to O concentrations



**Fig. 11.** Concentration profiles in one micro-tip analysed by APT after oxidation at 650 °C for 1000 h in flowing Ar-20%O<sub>2</sub>: (a) global and (b) enlargement on the low concentrations.



**Fig. 12.** Concentration profiles in one micro-tip analysed by APT after oxidation at 650°C for 1000 h in flowing synthetic air (a) global and (b) enlargement for the 60 first nanometres.

ratio ( $[Ti]/[O]=2.5$ ), zone B could also correspond to Ti<sub>2</sub>O or Ti<sub>3</sub>O lower oxides. These phases are not included in the TCTI1 database and, therefore, they do not appear in the computed Ti-O phase diagram of Fig. 1. Nevertheless, some experimental studies reported the Ti<sub>2</sub>O or Ti<sub>3</sub>O oxides as stable phases, in a not-well-defined domain below 600°C (see Fig. A1 of the appendices). Even if the oxidation experiments of this work were performed at 650 °C, these oxides could be formed at that temperature, considering the uncertainty about their stability domain, or they could also be formed during cooling, at the end of the oxidation.

Fig. 10b and Fig. 12 show the analyses for one sample oxidized in synthetic air. Concentration profiles obtained in the longitudinal direction are shown in Fig. 12. Three composition zones, namely C, D and E, can be observed. On the extreme surface of the APT tip, which corresponds to the inner part of the oxide scale, high concentrations of O, N and Ti were measured, suggesting an oxynitride phase (zone C). The presence of an oxynitride was also confirmed by a TEM/EELS study on a sample coming from the same batch [15]. This oxynitride could correspond to a solid solution between the iso-structural FCC TiO<sub>1±x</sub> and TiN<sub>1-x</sub> phases. This would explain the composition gradient observed in the zone C, since a solid solution can allow for a non-stoichiometric domain for both O and N.

Below the zone C, another region enriched in Ti and N and containing some O is observed (zone D). As the Ti to N concentrations ratio is equal to 1.6 and an Al depletion is noticed in this area (Al

solubility in Ti<sub>2</sub>N nitride is close to zero [33]), it could be a Ti<sub>2</sub>N nitride layer, 20 nm thick.

A third zone is composed of Ti, N and Al. As the aluminium content is close to the one of the alloy (slightly more than 10 at.%) with very little Mo, this should be the  $\alpha$ -Ti phase containing a great amount of nitrogen, up to 23 at.%. This value is larger than expected for the  $\alpha$ -Ti phase at 650 °C, which should dissolve about 11 at% at this temperature according to the phase diagram. It can be noted that the nitrogen solubility reaches 23 at% in pure  $\alpha$ -Ti at 1050°C [34]. Finally, Fig. 12 reveals that, at 20 or 30 nm below the oxide scale,  $\alpha$ -Ti(N) is saturated in nitrogen and it dissolves only 1 at.% of oxygen. This seems in contrast with the O concentration obtained by EPMA, which was about 10 at.% a few micrometers below the oxide scale, as seen in Fig. 7. To shed some light, a complementary TEM/EDS analysis of the alloy/oxide interface was performed for the Ti6242S oxidized in synthetic air and the result is shown in Fig. 13. At the interface, the nitrogen concentration (around 22 at.%) is in very good agreement with the value obtained by APT. Moreover, oxygen content is lower than 2 at.%, confirming also the APT results. However, going deeper into the alloy, for distances higher than 200 nm, a decrease in nitrogen content and a corresponding increase in oxygen, up to 10 at.%, are observed. This is consistent with the fact that oxygen is “rejected” deeper into the alloy when large amounts of nitrogen are present



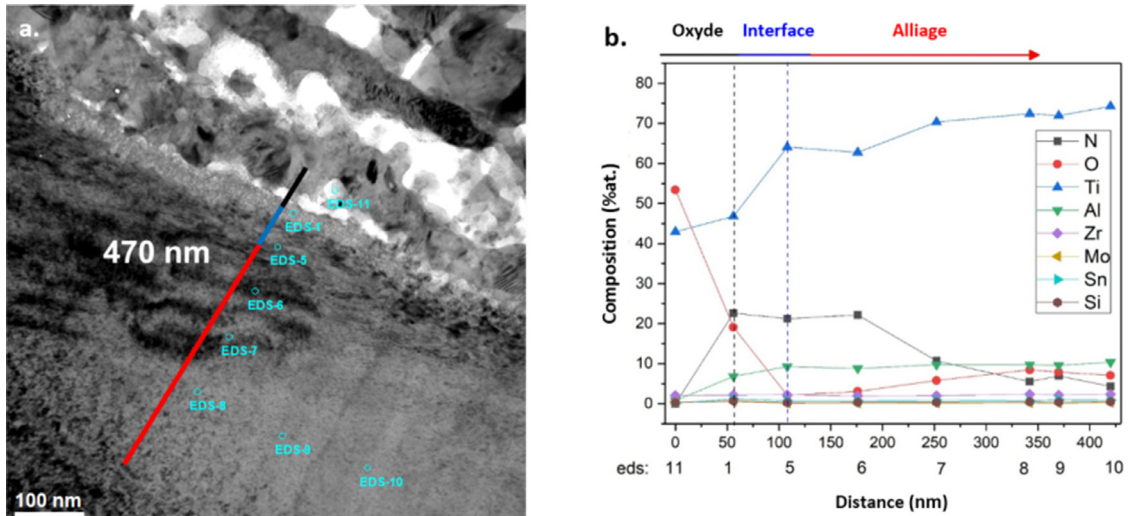


Fig. 13. (a) TEM observation and (b) relative EDS analysis of the alloy/oxide interface of the Ti6242S alloy oxidized at 650 °C for 1000 h in synthetic air.

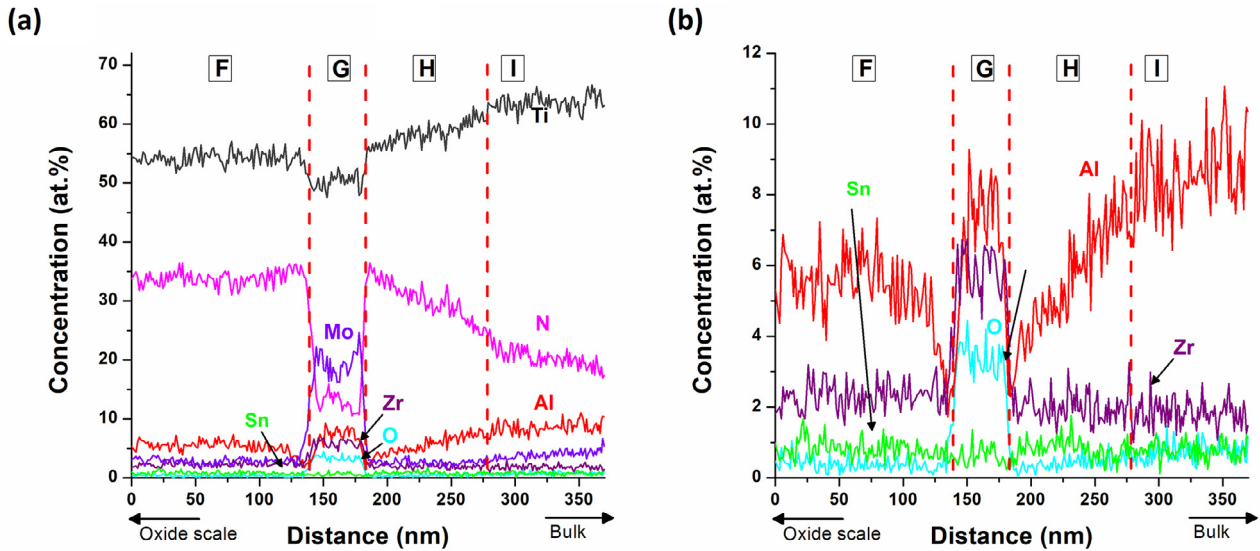


Fig. 14. Concentration profiles in the micro-tip analysed by APT and containing the  $\beta$ -phase after oxidation at 650 °C for 1000 h in flowing synthetic air: (a) global and (b) enlargement for lower concentrations.

at the alloy/oxide interface, or with the idea that N increases the chemical activity of O in the  $\alpha$ -Ti phase.

From the comparison of the previous results (Fig. 11 and Fig. 12), it appears that a high concentration of 29 at.% in oxygen is found in the  $\alpha$ -Ti(O) phase just under the oxide scale, for the Ti6242S oxidized in Ar-20%O<sub>2</sub> without nitrogen. This value is close to the solubility limit of oxygen in  $\alpha$ -Ti. On the contrary, an oxynitride, a titanium nitride Ti<sub>2</sub>N and a solid solution enriched in nitrogen formed during oxidation in synthetic air. The two latter phases contained low amounts of oxygen: 3-4 at.% for Ti<sub>2</sub>N and less than 1 at.% for  $\alpha$ -Ti(N). Then, it is shown that titanium nitride Ti<sub>2</sub>N and  $\alpha$ -Ti(N) could both act as a diffusion barrier for oxygen. This finding explain the decrease of oxygen dissolution within the alloy when oxidized in a nitrogen-rich atmosphere.

Among the three micro-tips prepared after oxidation in synthetic air, one (Fig. 10-c) presented a zone rich in titanium and molybdenum, corresponding to the zone G in Fig. 14. This Mo-rich

zone could be the BCC  $\beta$ -Ti phase, as molybdenum is known to segregate preferentially in this phase compared to the  $\alpha$ -Ti phase. Besides, no molybdenum (less than 0.1 at.%) was detected in the  $\alpha$ -Ti phase when present in the five other micro-tips. On both sides of  $\beta$ -Ti (zones F and H), a phase enriched in titanium and nitrogen formed, corresponding to the titanium nitride Ti<sub>2</sub>N, as already observed in the micro-tip related to synthetic air (Fig. 12). The presence of this nitride is confirmed by the element partitioning. Indeed, if the phase around the  $\beta$ -Ti phase was  $\alpha$ -Ti, tin and zirconium would be found equally in both phases and aluminium and oxygen would be strongly segregated in  $\alpha$ -Ti. However, it is seen from this micro-tip that these four elements were all segregated in the  $\beta$ -Ti phase. Therefore, it is most likely that the phase around  $\beta$ -Ti corresponded to titanium nitride Ti<sub>2</sub>N. It is worth noting that our analyses showed that oxygen solubility is higher in  $\beta$ -Ti than in Ti<sub>2</sub>N. A fourth zone, zone I, containing about 20 at.% of nitrogen and 11 at.% of aluminium is observed towards the alloy. Knowing

**Table 2**

Limit of solubility and partition coefficient of oxygen and nitrogen for the micro-tips analysed by APT after oxidation at 650°C for 1000 h in synthetic air and in Ar-20%O<sub>2</sub>.

Atmosphere	Synthetic air		Synthetic air with $\beta$ -Ti		Ar-20%O <sub>2</sub>		
	Ti <sub>2</sub> N	$\alpha$ -Ti(N)	Ti <sub>2</sub> N	$\beta$ -Ti(N)	TiO	$\alpha$ -Ti(O)	
Limit of solubility (at.%)	O	-	0.8	-	3	-	29
	N	-	22	-	14	-	-
Composition of phases (at.%)	O	4	0.8	0.4	3.3	46.9	24.5
	N	35	19.8	33.7	13.7	-	-
	Al	1.5	11.1	4.9	7.8	4.6	7.6
	Sn	2.5	0.7	0.8	0.7	3.5	0.9
	Zr	1.5	0.7	2.4	6.0	1.5	2.2
	Mo	-	-	3.1	17.2	0.2	0.3
	Si	0.3	0.3	-	-	1.3	0.8
	C	0.1	0.3	0.1	0.2	0	0.1
	H	0.1	0.2	-	-	1.5	0.1
	Ti	Bal.	Bal.	Bal.	Bal.	Bal.	Bal.
	Partition coefficients	O	Ti <sub>2</sub> N/ $\alpha$ -Ti(N): 5.0	Ti <sub>2</sub> N/ $\beta$ -Ti(N): 0.13	TiO/ $\alpha$ -Ti(O): 1.6	-	-
	N	Ti <sub>2</sub> N/ $\alpha$ -Ti(N): 2.0	Ti <sub>2</sub> N/ $\beta$ -Ti(N): 2.4	-	-	-	

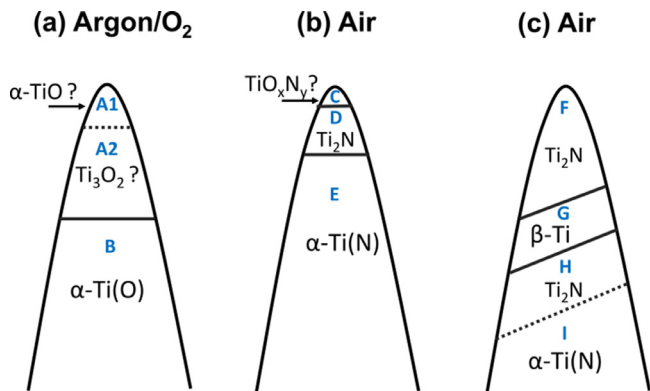


**Fig. 15.** Schema of micro-tips analysed by APT after oxidation at 650 °C for 1000 h in flowing (a) in Ar-20%O<sub>2</sub>, (b) and (c) in synthetic air.

that nitrogen solubility in pure titanium is 23 at.%, as observed before, and that aluminium content in the alloy is 10 at.%, this area is identified as a solid solution of titanium and nitrogen. However, it has to be mentioned that the interface between Ti<sub>2</sub>N titanium nitride and this solid solution is not obvious. 3D maps showed that each zone, identified as Ti<sub>2</sub>N and  $\alpha$ -Ti(N), are single phased as only one contrast was observed.

From these analyses, it was possible to determine the contents of oxygen and nitrogen within the identified phases and their partition coefficients. It is summarised in Table 2.

Finally, a schematic representation of the three studied micro-tips, with the attempt for phase identification, is shown in Fig. 15.

### 3.3. Thermodynamic data and evaluation of the TCTI1 database

The results obtained with APT analyses were compared to thermodynamic calculations made with the TCTI1 database using the Thermo-Calc software. TCTI1 deals with Ti-based and TiAl alloys and includes oxygen and nitrogen elements. The measured chemical compositions were used as input data to determine if the phases identified from APT analyses were predicted by Thermo-Calc/TCTI1 as thermodynamically stable. Results are shown in Table 3.

For oxidation in Ar-20%O<sub>2</sub>, thermodynamic calculations in the zone A (A1 and A2) resulted in a mixture of intermediate titanium oxides, namely  $\alpha$ -TiO and  $\beta$ -TiO<sub>1±x</sub>, consistently with the

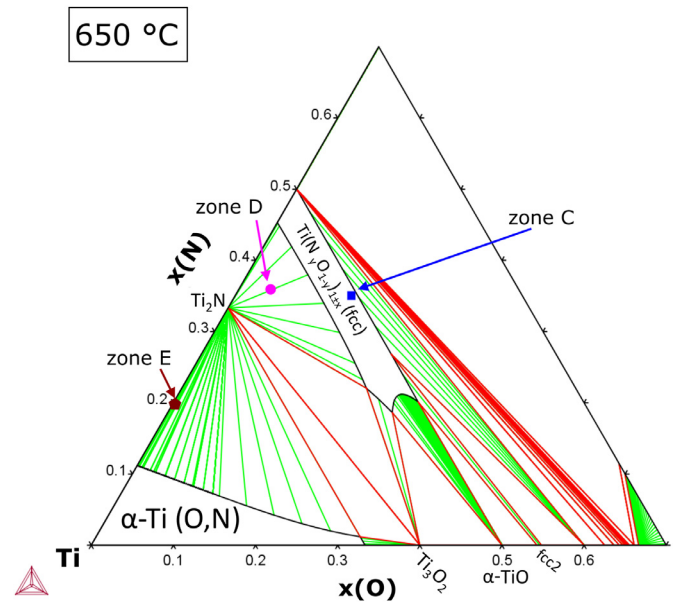


**Fig. 16.** Ternary Ti-N-O phase diagram computed at 650°C (computations with the TCTI1 database from Thermo-Calc).

APT analyses. However, the calculations predict the presence of other phases: alumina, monoclinic zirconia, intermetallic phases and silicides. This is not in agreement with the experimental results since none of these phases were detected. The dissolution of small amounts of Al, Sn, Si, Mo, and Zr in titanium oxides, which is shown experimentally, is not taken into account in the TCTI1 database. Therefore, the appearance of the other phases is likely an artefact.

For the second zone (B), the major phase is  $\alpha$ -Ti enriched in oxygen, which is consistent with APT results. However, quite surprisingly, in addition to Ti and O, only a low amount of Zr is present in  $\alpha$ -Ti, according to the calculations. The absence of Al in this phase is particularly surprising. The thermodynamic calculations predict the formation of  $\alpha$ -Ti<sub>3</sub>Al and Ti<sub>3</sub>AlO, but these phases were not detected during characterisations. Other phases (silicides and intermetallics) were also predicted but were not observed experimentally.

**Table 3**

Comparison of experimental data from APT analyses and thermodynamic calculations (Thermo-Calc/TCTI1 database).

Atmos-phere	Compositions by APT (%at)	Phases	Proportion of phases from TC calculations (%mol)	Composition of phases from TC calculations (%mol)
Ar-20%O <sub>2</sub>	<b>A zone</b> 47O-41Ti-4.6Al-3.5Sn-1.5Zr-1.5H-1.3Si-0.15Mo-0.022C	$\alpha$ -TiO / FCC-TiO <sub>1±x</sub> + Ti <sub>3</sub> O <sub>2</sub>	56.2% $\alpha$ -TiO 16% FCC-TiO <sub>1±x</sub> 12.1% Corundum Al <sub>2</sub> O <sub>3</sub> 7.5% Ti <sub>6</sub> Sn <sub>5</sub> 4.5% ZrO <sub>2_mono</sub> 3.7% M <sub>5</sub> Si <sub>3_D88</sub>	50Ti-50O 46Ti-54O 2 Ti-38Al-60O Ti <sub>6</sub> Sn <sub>5</sub> ZrO <sub>2</sub> 59Ti-4Mo-35Si-2Sn
	<b>B zone</b> 64Ti-25O-7.6Al-2.2Zr-0.86Sn-0.84Si-0.27Mo-0.13C-0.10H	$\alpha$ -Ti(O)	61% $\alpha$ -Ti (hcp) 21% $\alpha_2$ -Ti <sub>3</sub> Al 11% Ti <sub>3</sub> AlO <sub>101</sub> 2.2% M <sub>5</sub> Si <sub>3_D88#2</sub> 2.3% M <sub>5</sub> Si <sub>3_D88#1</sub> 1.5% AlZr 1% FCC-TiO <sub>1±x</sub>	66Ti-1Zr-33O 67Ti-23Al-10O 60Ti-18Al-22O 41Zr-21Ti-38Sn 63Ti-36Si-1Sn 50Al-50Zr 54Ti-16C-30O
Synthetic air	<b>C &amp; D zones</b> 55Ti-33N-2.1Al-1.2Zr-2.2Sn-5.6O-0.077Si-0.80C-0.086H	TiO <sub>x</sub> N <sub>y</sub> + Ti <sub>2</sub> N	51% FCC-Ti(N <sub>y</sub> O <sub>1-y</sub> ) <sub>1±x</sub> 34% Ti <sub>2</sub> N_C4 (Ti <sub>2</sub> N) 6.1% M <sub>5</sub> Si <sub>3_D88#2</sub> 3.6% FCC-Ti(N <sub>y</sub> O <sub>1-y</sub> ) <sub>1±x</sub> 5.3% Corundum (Al <sub>2</sub> O <sub>3</sub> ) 0.40% M <sub>5</sub> Si <sub>3_D88#1</sub>	55Ti-42N-3O 67Ti-33N 42Ti-21Zr-37Sn 51Ti-20C-27O-2N 40Al-60O 63Ti-12Sn-25Si
	<b>E zone</b> 66Ti-20N-11Al-0.74Zr-0.66Sn-0.87O-0.30Si-0.29C-0.22H	$\alpha$ -Ti(N)	55% Ti <sub>2</sub> N_C4 (Ti <sub>2</sub> N) 29% AlTi <sub>3_D019#2</sub> ( $\alpha_2$ -Ti <sub>3</sub> Al) 9% AlNTi <sub>3</sub> (Ti <sub>3</sub> AlN) 2.8% AlTi <sub>3_D019#1</sub> ( $\alpha_2$ -Ti <sub>3</sub> Al) 1.1% Al <sub>3</sub> Zr <sub>2</sub> 1.8% Ti <sub>2</sub> AlC 46% Ti <sub>2</sub> N_C4 (Ti <sub>2</sub> N)	67Ti-33N 71Ti-27Al-3.0O 60Ti-20Al-20N 74Ti-14Al-11Sn-1Zr 60Al-40Zr 50Ti-25Al-25C
Synthetic air ( $\beta$ phase)	<b>F &amp; H zones</b> 55Ti-34N-4.9Al-3.1Mo-2.4Zr-0.83Sn-0.37O-0.055C	Ti <sub>2</sub> N	42% FCC-Ti(N <sub>y</sub> O <sub>1-y</sub> ) <sub>1±x</sub> 4.2% Cr <sub>3</sub> Si_A15 4.2% C14_Laves 1.9% M <sub>5</sub> Si <sub>3_D88</sub> 1.8% Al <sub>3</sub> Ti_D022 (TiAl <sub>3</sub> )	67Ti-33N 54.7Ti-44.8N-0.5O 60Mo-15Ti-25Al 61Al-33Zr-6Mo 53 Zr- 44Sn-3Ti 17 Ti-65Al-18Mo
	<b>G zone</b> 51Ti-14N-7.8Al-17Mo-6.0Zr-0.69Sn-3.3O-0.23C	$\beta$ -Ti	29% BCC_B2 ( $\beta$ -Ti) 33% Ti <sub>2</sub> N_C4 (Ti <sub>2</sub> N) 12% Cr <sub>3</sub> Si_A15 11% HCP_A3#3+11% HCP_A3#2 ( $\alpha$ -(Ti,Zr)) 1.9% M <sub>5</sub> Si <sub>3_D88-1.8%</sub> FCC_B1	48Ti-35Mo-16Al-0.64Zr 67Ti-33N 55Mo-25Al-20Ti 39Zr-39Ti-21N-0.12O+ 66Ti-27O-4.5Zr-2.6N 50Zr-13Ti-37Sn
	<b>I zone</b> 64Ti-20N-8.8Al-4.2Mo-1.8Zr-0.80Sn-0.83O-0.066C	$\alpha$ -Ti(N)	59% Ti <sub>2</sub> N_C4 (Ti <sub>2</sub> N) 20% AlTi <sub>3_D019#2</sub> ( $\alpha_2$ -Ti <sub>3</sub> Al) 17% BCC_B2#1 ( $\beta$ -Ti) 2.1% M <sub>5</sub> Si <sub>3_D88-</sub> 1.5% AlZr 0.4% Ti <sub>3</sub> AlC <sub>2</sub>	67Ti-33N 71Ti-24Al-5O 75Ti-22Mo-2Al-1.0Zr 47Zr-16Ti-37Sn 50 Al-50Zr 60Ti-20Al-20C

As a guide for the eye, the compositions of the zones identified for the first sample oxidized in air (zones C, D and E) are reported on the computed Ti-N-O ternary phase diagram (at 650 °C) in Fig. 16, on the basis of the measured oxygen and nitrogen contents. A solid solution between FCC  $\beta$ -TiO<sub>1±x</sub> and FCC TiN<sub>1-x</sub> is present in this ternary system, indicated as Ti(N<sub>y</sub>O<sub>1-y</sub>)<sub>1±x</sub>. The composition of the zone C falls in this domain. However, as previously said, the ternary Ti-N-O system is not assessed in the TCTI1 database but only extrapolated from the binaries. Therefore, the phase boundaries of the FCC solid solution are likely not well described. Calculations were made considering the complete chemical compositions determined by APT (Table 3). For the zones C and D, two major phases were obtained. The first one is the FCC Ti(N<sub>y</sub>O<sub>1-y</sub>)<sub>1±x</sub> solid solution, containing 42 at.% nitrogen and only 3 at.% oxygen. The second phase is the Ti<sub>2</sub>N titanium nitride. According to the TCTI1 database, Ti<sub>2</sub>N contains only titanium and nitrogen, whereas our observations showed some O, Sn, Zr, Al and Si dissolution. Consequently, the remaining composition is artificially enriched in these elements, promoting the formation of silicides. In addition, a second FCC-Ti(N<sub>y</sub>O<sub>1-y</sub>)<sub>1±x</sub> solid solution, rich in oxy-

gen and carbon, is predicted. This is likely due to the fact that this solid solution is not well described. For the E- zone, identified as  $\alpha$ -Ti(N), two major phases are predicted by Thermo-Calc: Ti<sub>2</sub>N and  $\alpha_2$ -Ti<sub>3</sub>Al. The prediction of the Ti<sub>2</sub>N phase was anticipated by the discussion of the previous section since, according to the database, the nitrogen solubility in  $\alpha$ -Ti is limited at 11 at.% at 650 °C. On the contrary, our results seem to indicate that this value is larger, around 20 at.%. More surprisingly, the second predicted phase is not  $\alpha$ -Ti(N), but  $\alpha_2$ -Ti<sub>3</sub>Al. Once again, in this study, this phase was not detected experimentally.

For the micro-tip containing  $\beta$ -Ti after oxidation in synthetic air, thermodynamic calculations in the zones F, H and I (corresponding to Ti<sub>2</sub>N and  $\alpha$ -Ti(N)) were similar to those already obtained for oxidation in synthetic air. In the zone G, corresponding to  $\beta$ -Ti, the calculations predict Ti<sub>2</sub>N,  $\beta$ -Ti and  $\alpha$ -Ti. Contrary to the experiment, the computations do not show nitrogen dissolution in the  $\beta$ -Ti and, consequently, Ti<sub>2</sub>N is obtained.

In summary, a fair agreement is obtained between the thermodynamic calculations and the experimental results, but some significant discrepancies can be highlighted:

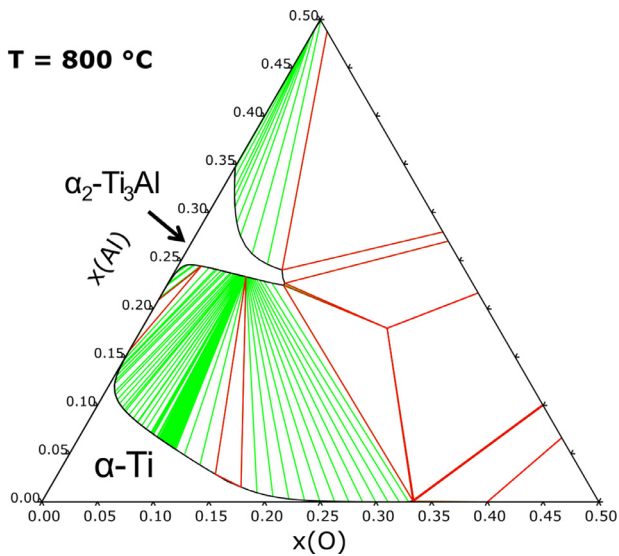


**Fig. 17.** Ti-Al-O phase diagram at 800°C (computations with the TCTI1 database from Thermo-Calc).

- 1) In the titanium oxide regions (zone A), phases such as silicide and intermetallic are predicted because of an incomplete thermodynamic description of various Ti oxides, for which the solubility of other elements (Al, Zr, Sn...) is not taken into account.
- 2) Similar discrepancies are obtained for the nitride regions because the description of the N-containing systems is not complete in the database. For example, the description of the titanium nitride  $Ti_2N$  only contains Ti and N, whereas APT analyses revealed that Al and O can dissolve within it. Moreover, our APT results indicate that the nitrogen solubility in  $\alpha$ -Ti, at 650 °C, is larger than expected by the database.
- 3) Considerable amounts of the  $\alpha_2$ - $Ti_3Al$  phase (21-29 mol.%) are predicted by the calculations, but this phase was not observed in this study.

The last point deserves further discussion, since  $\alpha_2$ - $Ti_3Al$  is fragile and it can have a detrimental effect on fracture toughness and fatigue. Previous works actually suggest that oxygen stabilizes the  $\alpha_2$ - $Ti_3Al$  phase within the  $\alpha$ -Ti [25,26]. Bagot *et al.* combined TEM and APT to characterize a TA6V alloy, oxidized at 800°C for 24h [25], and their results showed a considerable amount of  $\alpha_2$ - $Ti_3Al$ , whose composition was clearly identifiable [25]. First, the Al concentrations observed for the  $\alpha_2$ - $Ti_3Al$  regions were higher than 20 at.% [25], whereas in our examinations the Al concentration never exceeds 10 at.%. Second, Bagot *et al.* observed a clear partition of oxygen between the  $\alpha$ -Ti and  $\alpha_2$ - $Ti_3Al$  phases, in agreement with the solubility limits: around 10 at.% [35,36] in  $\alpha_2$ - $Ti_3Al$  and 30 at.% in  $\alpha$ -Ti. It can seem puzzling that oxygen causes the precipitation of the  $\alpha_2$ - $Ti_3Al$ , despite the fact that the oxygen solubility in this phase (11 at.% [35,36]) is lower than that in  $\alpha$ -Ti (33 at.%). Fig. 17 shows the computed (TCTI1 database) ternary Ti-Al-O phase diagram at 800°C. The orientation of the tie-lines in the biphasic  $Ti_3Al(O)$ -Ti(O) domain exhibits an inversion of direction, for  $x(O) \approx 7$  at.%. Below this value, the oxygen preferentially partition in the  $\alpha_2$ - $Ti_3Al$ ; when the overall oxygen content exceeds 7 at.%, oxygen is present in higher concentration in  $\alpha$ -Ti. A possible explanation is that the driving force for  $\alpha_2$ - $Ti_3Al$  precipitation is higher when oxygen is present in low concentration, hence when it starts diffusing through the alloy. The computed phase diagram at 650 °C (see appendix Fig. A5) is similar to that at 800°C. However, it is hard to compare our study with that of Bagot *et al.* [25], since they concern different alloy composition, temperature

and duration. However, these results highlight that the  $\alpha$ -Ti(O)/ $\alpha_2$ - $Ti_3Al(O)$  equilibria are not clear yet and further investigations will be necessary to fill the gap.

#### 4. Conclusions

The effect of nitrogen on the oxidation behaviour of Ti-6Al-2Sn-4Zr-2Mo-0.1Si Ti-based alloy was studied at 650 °C for 1000 h, thanks to oxidation treatments in synthetic air ( $N_2$ -20% $O_2$ ) and in a mixture of Ar-20% $O_2$ , i.e. with the same oxygen partial pressure but without nitrogen. Results showed that nitrogen greatly decreases global oxidation kinetics by decreasing both the oxide scale growth and the oxygen dissolution within the alloy.

For the first time, the APT technique was successfully applied to the characterization of the Ti-based alloy/oxide interface. Thanks to these APT analyses, oxygen and nitrogen contents (together with those of the metallic elements) were determined in the observed oxides, oxynitride, nitrides and alloy.

According to the APT results, the decrease of the oxidation kinetics in presence of nitrogen is due to the formation of an oxynitride/nitride ( $Ti_2N$ ) layer and of a nitrogen-rich Ti-based solid solution, which both act as diffusion barrier. Moreover, our results indicate that the nitrogen solubility in  $\alpha$ -Ti at 650 °C is around 20 at.%, i.e. close to the maximum value which is generally attributed only to high temperature (around 1060°C). For oxidation in Ar-20% $O_2$ , intermediate titanium oxides were identified between the  $TiO_2$  scale and the  $\alpha$ -Ti phase, the latter being enriched in oxygen.

To compare experimental data to thermodynamic ones, calculations with Thermo-Calc software using TCTI1 database were performed. The phases identified from APT analyses were in fair agreement with those predicted by equilibrium calculations, but some important discrepancies were noticed. Most of these came from the fact that the solubilities of alloy elements (Al, Zr, Mo...) are not described for several titanium nitrides and oxides, leading to artificial stabilisation of phases (intermetallic, silicides...) which were not observed experimentally. Another important discrepancy between calculations and experimental results is related to the  $\alpha_2$ - $Ti_3Al$  phase, which is predicted by the calculations, in considerable amounts (> 20 mol.%), for all the regions below the oxide scale, but it was never observed in the present work. Therefore, it seems that the  $\alpha$ -Ti(O)/ $\alpha_2$ - $Ti_3Al(O)$  phase equilibria need to be further investigated and their thermodynamic models have to be reviewed together with their kinetics of formation. Advanced characterizations techniques such as APT can be good assets for these studies.

#### Declaration of Competing Interest

The authors declare that they have no known competing financial interests or personal relationships that could have appeared to influence the work reported in this paper.

#### Acknowledgements

This work was supported by the French National Research Agency through the project ANR DUSTI in partnership between Airbus, Airbus Group Innovations, Aubert and Duval, Liebherr Toulouse Aerospace, Institut Pprime, Institut Jean Lamour and CIR-IMAT Laboratory. The authors would like to thank Alessandro Puigliara for the TEM analysis and Claudie Josse for preparation of the TEM samples by FIB (Castaing microanalysis center, Toulouse, France). The authors also acknowledge financial support from the CNRS-CEA "METSA" French network (FR CNRS 3507) for the APT experiments at IM2NP.

Appendices

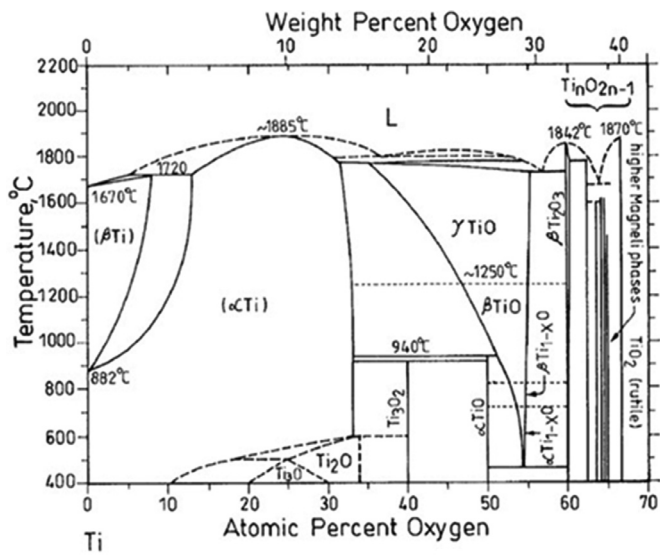


Fig. A1. Experimental Ti-O phase diagram as reported by Murray and Wriedt [31].

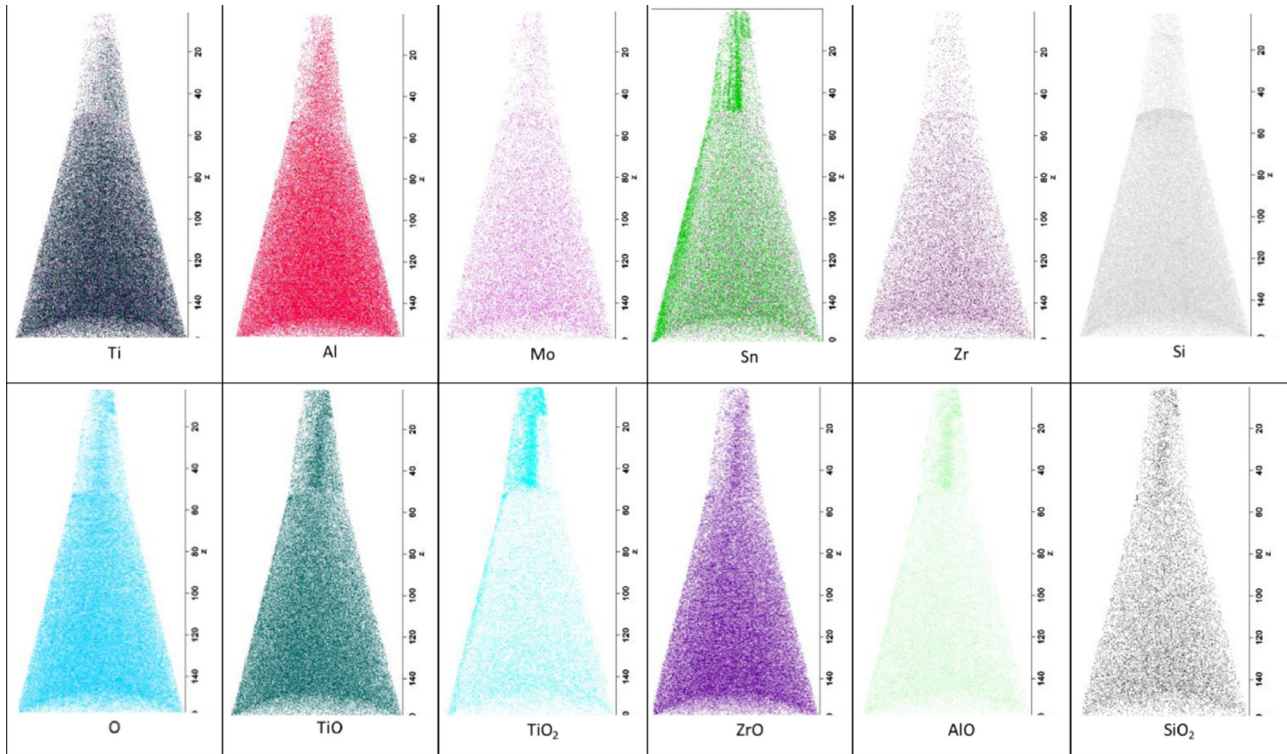
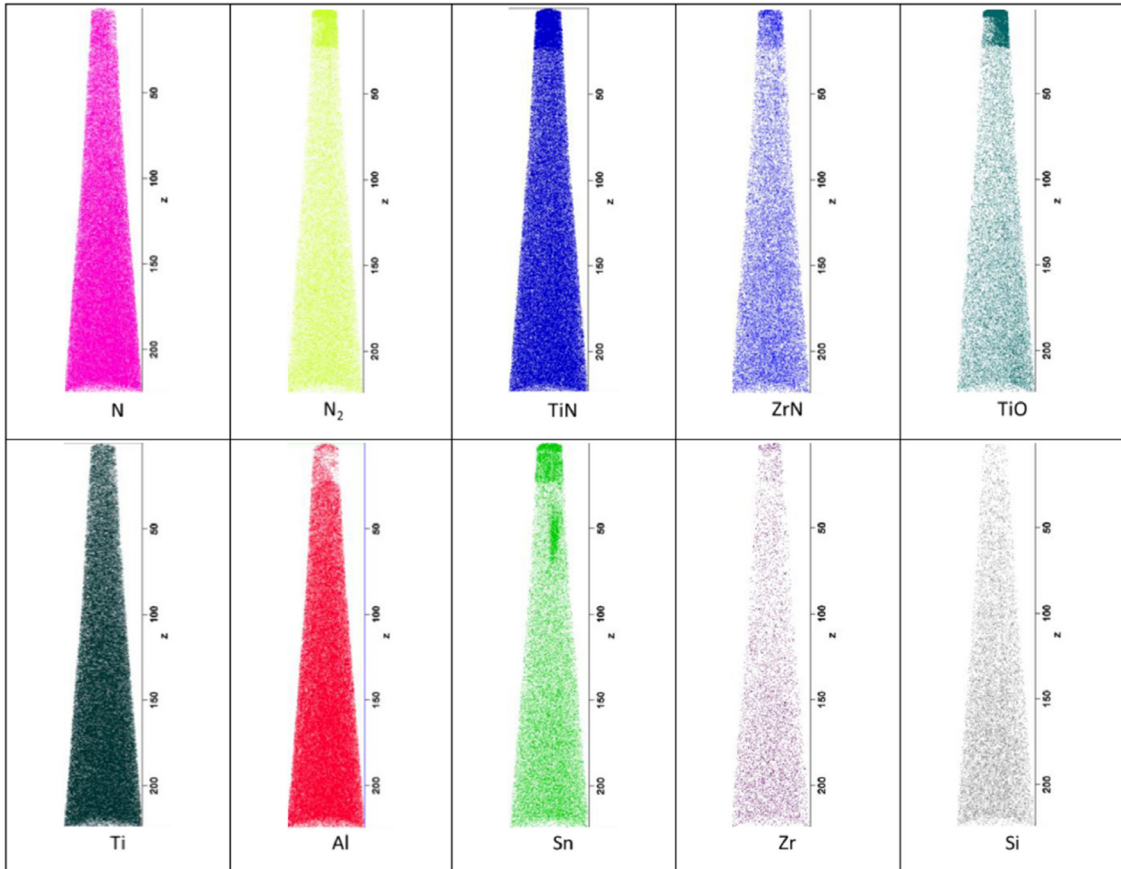


Fig. A2. Elemental maps of the micro-tip extracted from the sample oxidized in Ar-20%O<sub>2</sub>.



**Fig. A3.** Elemental maps of the micro-tip extracted from the sample oxidized in synthetic air (presenting the zones C, D and E).

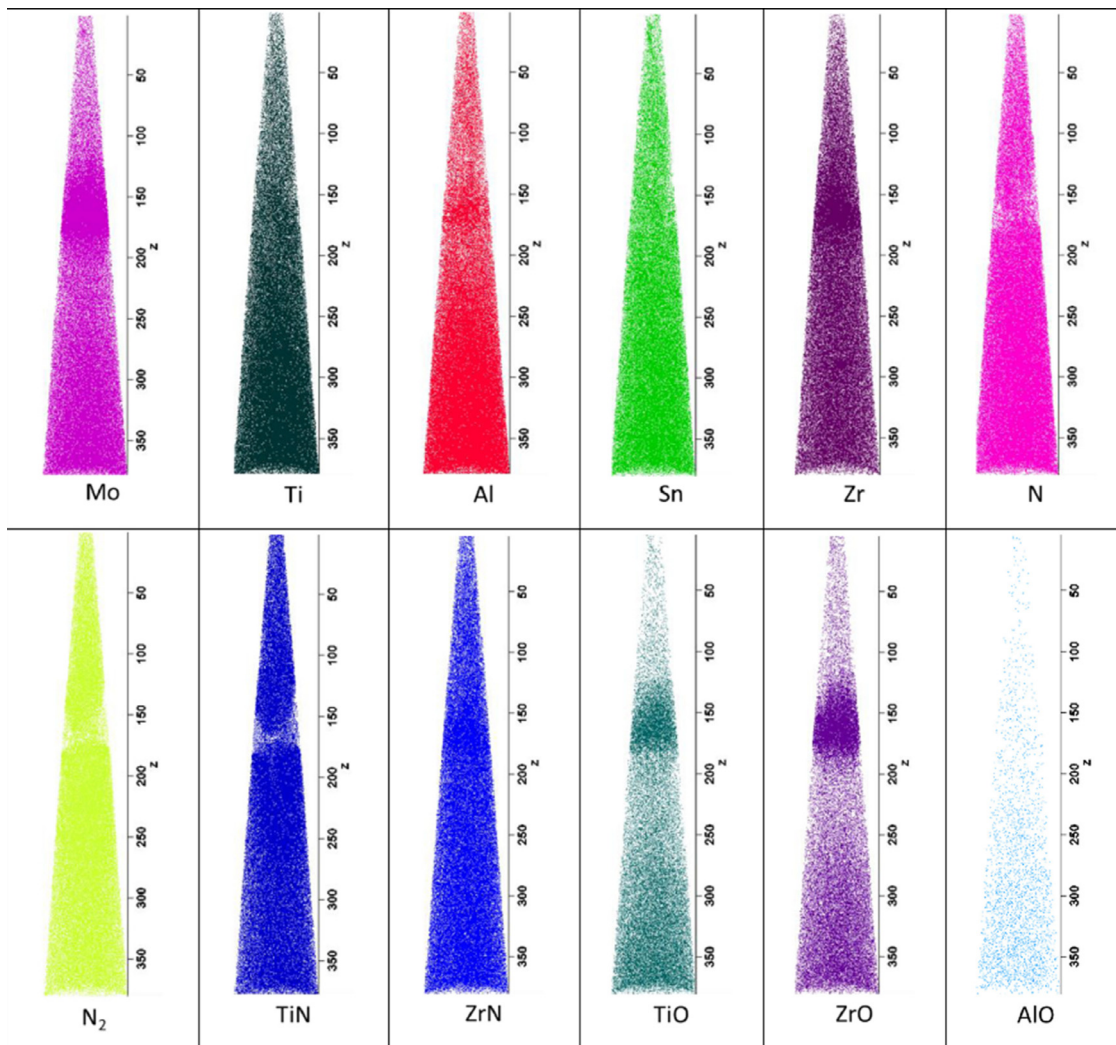


Fig. A4. Elemental maps of the micro-tip extracted from the sample oxidized in synthetic air (presenting the zones F, G, H and I).

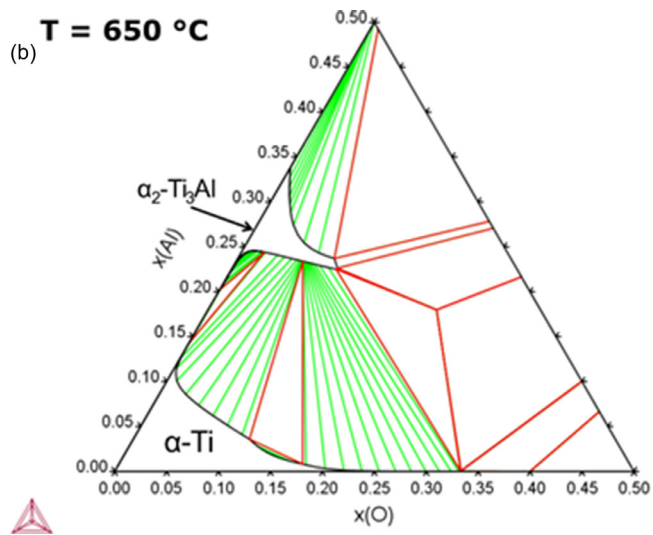


Fig. A5. Ternary Ti-Al-O phase diagram at 650 °C, computed with the TCT11 database.

## References

- [1] D. Satko, J. Shaffer, J. Tiley, S. Semiatin, A. Pilchak, S. Kalidindi, Y. Kosaka, M. Glavicic, A. Salem, Effect of microstructure on oxygen rich layer evolution and its impact on fatigue life during high-temperature application of  $\alpha/\beta$  titanium, *Acta Materialia* 107 (2016) 377–389.
- [2] W.L. Finlay, J.A. Snyder, Effects of three interstitial solutes (nitrogen, oxygen, and carbon) on the mechanical properties of high-purity, alpha titanium, *JOM* 2 (2) (1950) 277–286.
- [3] H. Fukai, H. Iizumi, K. Minakawa, C. Ouchi, The effects of the Oxygen-enriched Surface Layer on Mechanical Properties of  $\alpha+\beta$  Type Titanium Alloys, *ISIJ International* 45 (1) (2005) 133–141.
- [4] J.-P. Bars, D. David, E. Etchessahar, J. Debuigne, Titanium  $\alpha$ - nitrogen solid solution formed by high temperature nitriding: diffusion of nitrogen, hardness, and crystallographic parameters, *Metall Mater Trans A* 14 (8) (1983) 1537–1543.
- [5] A.M. Chaze, C. Coddet, The role of nitrogen in the oxidation behaviour of titanium and some binary alloys, *Journal of the Less Common Metals* 124 (1) (1986) 73–84.
- [6] C. Dupressoire, A. Rouaix-Vande Put, P. Emile, C. Archambeau-Mirguet, R. Peraldi, D. Monceau, Effect of Nitrogen on the Kinetics of Oxide Scale Growth and of Oxygen Dissolution in the Ti6242S Titanium-Based Alloy, *Oxid Met* 87 (3) (2017) 343–353.
- [7] K.N. Strafford, A comparison of the high temperature nitridation and oxidation behaviour of metals, *Corrosion Science* 19 (1) (1979) 49–62.
- [8] X. Pan, M.-Q. Yang, X. Fu, N. Zhang, Y.-J. Xu, Defective TiO<sub>2</sub> with oxygen vacancies: synthesis, properties and photocatalytic applications, *Nanoscale* 5 (9) (2013) 3601–3614.
- [9] A.M. Chaze, C. Coddet, Influence of alloying elements on the dissolution of oxygen in the metallic phase during the oxidation of titanium alloys, *J Mater Sci* 22 (4) (1987) 1206–1214.

- [10] A.M. Chaze, C. Coddet, Influence of chromium on the oxidation of titanium between 550° and 700°C, *Oxid Met* 21 (3) (1984) 205–231.
- [11] A.M. Chaze, C. Coddet, Influence of silicon on the oxidation of titanium between 550 and 700°C, *Oxid Met* 27 (1) (1987) 1–20.
- [12] J. Rakowski, D. Monceau, F.S. Pettit, G.H. Meier, R.A. Perkins, *Microscopy of Oxidation 2: Proceedings of the Second International Conference on the Microscopy of Oxidation Held at Selwyn College, the University of Cambridge, 1993*, p. 476–487.
- [13] S. Becker, A. Rahmel, M. Schorr, M. Schütze, Mechanism of isothermal oxidation of the inter-metallic TiAl and of TiAl alloys, *Oxid Met* 38 (5) (1992) 425–464.
- [14] A. Kanjer, V. Optasanu, M. M. Marco de Lucas, O. Heintz, N. Geoffroy, M. Francois, P. Berger, T. Montesin, L. Lavis, et al., Improving the high temperature oxidation resistance of pure titanium by shot-peening treatments, *Surface and Coatings Technology* 343 (2017) 93–100.
- [15] I. Abdallah, C. Dupressoire, L. Laffont, D. Monceau, et al., Vande Put, STEM-EELS identification of TiOXNY, TiN, Ti<sub>2</sub>N and O, N dissolution in the Ti2642S alloy oxidized in synthetic air at 650 °C, *Corrosion Science* 153 (2019) 191–199.
- [16] X. Tan, Y. Kok, Y. J. Tan, M. Descoins, D. Mangelinck, S. B. Tor, K. Leona, C. K. Chua, et al., Graded microstructure and mechanical properties of additive manufactured Ti–6Al–4V via electron beam melting, *Acta Materialia* 97 (2015) 1–16.
- [17] X. Tan, Y. Kok, W. Toh, J. Tan, M. Descoins, M. Mangelinck, S.B Tor, K. Leong, C. K. Chua, et al., Revealing martensitic transformation and  $\alpha/\beta$  interface evolution in electron beam melting three-dimensional-printed Ti-6Al-4V, *Sci Rep* 6 (1) (2016) 26039.
- [18] N. Sridharan, Y. Chen, P. Nandwana, R.M. Ulfing, D.J. Larson, S.S. Babu, On the potential mechanisms of  $\beta$  to  $\alpha' + \beta$  decomposition in two phase titanium alloys during additive manufacturing: a combined transmission Kikuchi diffraction and 3D atom probe study, *J Mater Sci* 55 (4) (2020) 1715–1726.
- [19] J. Coakley, V. A. Vorontsov, N. G. Jones, A. Radecka, P. A. J. Bagot, K. C. Littrell, R. K. Heenan, F. Hu, A. P. Magyar, D. C. Bell, D. Dye, et al., Precipitation processes in the Beta-Titanium alloy Ti–5Al–5Mo–5V–3Cr, *Journal of Alloys and Compounds* 646 (2015) 946–953.
- [20] R.P. Kollis, A.A. Herzing, S. Ankem, Characterization of yttrium-rich precipitates in a titanium alloy weld, *Materials Characterization* 122 (2016) 30–35.
- [21] A. Radecka, J. Coakley, V. A. Vorontsov, T. L. Martin, P. A. J. Bagot, M. P. Moody, D. Rugg, D. Dye, et al., Precipitation of the ordered  $\alpha_2$  phase in a near- $\alpha$  titanium alloy, *Scripta Materialia* 117 (2016) 81–85.
- [22] J. Coakley, A. Radecka, D. Dye, P.A.J. Bagot, T.L. Martin, T.J. Prosa, Y. Chen, H.J. Stoneb, D.N. Seidman, D. Isheim, Characterizing nanoscale precipitation in a titanium alloy by laser-assisted atom probe tomography, *Materials Characterization* 141 (2018) 129–138.
- [23] M. Yan, M.S. Dargusch, T. Ebel, M. Qian, A transmission electron microscopy and three-dimensional atom probe study of the oxygen-induced fine microstructural features in as-sintered Ti–6Al–4V and their impacts on ductility, *Acta Materialia* 68 (2014) 196–206.
- [24] D. Rugg, T.B. Britton, J. Gong, A.J. Wilkinson, et P.A.J. Bagot, In-service materials support for safety critical applications – A case study of a high strength Ti-alloy using advanced experimental and modelling techniques, *Materials Science and Engineering: A* 599 (2014) 166–173.
- [25] P.A.J. Bagot, A. Radecka, A.P. Magyar, Y. Gong, D.C. Bell, G.D.W. Smith, M.P. Moody, D. Dye, D. Rugg, The effect of oxidation on the subsurface microstructure of a Ti-6Al-4V alloy, *Scripta Materialia* 148 (2018) 24–28.
- [26] H.M. Gardner, A. Radecka, D. Rugg, D.E.J. Armstrong, M.P. Moody, P.A.J. Bagot, A study of the interaction of oxygen with the  $\alpha_2$  phase in the model alloy Ti–7wt%Al, *Scripta Materialia* 185 (2020) 111–116.
- [27] K. Thompson, D. Lawrence, D.J. Larson, J.D. Olson, T.F. Kelly, B. Gorman, In situ site-specific specimen preparation for atom probe tomography, *Ultramicroscopy* 107 (2–3) (2007) 131–139.
- [28] D. Larson, D.T. Foord, A.K. Petford-Long, H. Liew, M.G. Blamire, A. Cerezo, G.D.W. Smith, Field-ion specimen preparation using focused ion-beam milling, *Ultramicroscopy* 79 (1) (1999) 287–293.
- [29] H. Lukas, S.G. Fries, B. Sundman, *Computational Thermodynamics: The Calphad Method*, 1st ed., Cambridge University Press, USA, 2007.
- [30] Y. Cadoret, N. Vaché, D. Monceau, B. Dod, Modeling the oxidation kinetics of titanium alloys: Review, method and application to Ti-64 and Ti-6242s alloys, *Corr. Sc.* 178 (2021) January.
- [31] J.L. Murray, H.A. Wriedt, The O-Ti (Oxygen-Titanium) System, *Bulletin of Alloy Phase Diagrams* 8 (1987) 148–165.
- [32] D. Samélor, L. Baggetto, R. Laloo, V. Turq, A. Gleizes, T. Duguet, D. Monceau, C. Vahlas, Efficient, durable protection of the Ti6242S titanium alloy against high-temperature oxidation through MOCVD processed amorphous alumina coatings, *J Mater Sci* 55 (11) (2020) 4883–4895.
- [33] J.C. Schuster, J. Bauer, The ternary system titanium-aluminum-nitrogen, *Journal of Solid State Chemistry* 53 (2) (1984) 260–265.
- [34] H.A. Wriedt, J.L. Murray, The N-Ti (Nitrogen-Titanium) system, *Bulletin of Alloy Phase Diagrams* 8 (4) (1987) 378–388.
- [35] S. Das, The Al-O-Ti (Aluminum-oxygen-titanium) system, *JPE* 23 (6) (2002) 525–536.
- [36] C.Y. Jones, W.E. Luecke, E. Copland, Neutron diffraction study of oxygen dissolution in  $\alpha_2$ -Ti<sub>3</sub>Al, *Intermetallics* 14 (1) (2006) 54–60.